An evaluation of microphysics in a numerical model using Doppler velocity measured by ground-based radar for application to the EarthCARE satellite

Woosub Roh[1], Masaki Satoh[1], Yuichiro Hagihara[2], Hiroaki Horie[2], Yuichi Ohno[2], and Takuji Kubota[3]

[1]Atmosphere and Ocean Research Institute, The University of Tokyo, Kashiwa, Chiba 277-8564, Japan
[2]National Institute of Information and Communications Technology, Koganei, Japan
[3]Earth Observation Research Center, Japan Aerospace Exploration Agency, Tsukuba, Ibaraki, Japan

Correspondence to: Woosub Roh (ws-roh@aori.u-tokyo.ac.jp)

Abstract. The Cloud Profiling Radar (CPR) of the Earth Cloud, Aerosol and Radiation Explorer (EarthCARE) has a new capability to observe the Doppler velocity related to the vertical air motion of the terminal velocity of hydrometeors. The new observation from space will be used to evaluate and improve the model. Before the launch of EarthCARE, we need to develop a methodology for using the CPR data for model evaluations. In this study, we evaluated simulated data by a stretched version of the global non-hydrostatic model over Japan with a ground-based CPR using an instrument design similar to the EarthCARE CPR. We chose two cases with different precipitation events in September 2019 using two cloud microphysics schemes. We introduced the categorization method for evaluating microphysics using Doppler velocity. The results show that the liquid and solid phases of hydrometeors are divided in Doppler velocity, and the model's terminal velocities of rain, snow, and graupel categories can be evaluated with the observation. The results also show that the choice of microphysics scheme has a more significant impact than the dependence on precipitation cases. We discussed the application of the EarthCARE-like simulation results using a satellite simulator.

1 Introduction

The Satellite data have been used to evaluate and improve clouds and precipitation of global circulation models (GCMs). Recently, Global storm resolving models (GSRMs, Satoh et al. 2019; Stevens et al. 2019) have been used to produce more detailed simulations of mesoscale convective systems with km-scale horizontal mesh, which is much finer resolution than typical GCMs. GSRMs are expected to reduce the uncertainty of GCMs due to the cumulus parameterization. GSRMs implement cloud microphysics schemes to achieve realistic simulations of clouds and precipitation by considering the detailed process of hydrometeors, such as nucleation, coalescence, and precipitation in the model. Most of the horizontal sampling of the active satellite sensors is less than 5 km, which is comparable to the horizontal resolution of GSRMs. Therefore, it is possible to directly compare the satellite data and the results of GSRMs without any subgrid assumption. Several studies have

30   evaluated and improved microphysics using satellite active sensor data (e.g., Roh and Satoh 2014; Roh et al. 2017; Ikuta et al. 2021).

New observations, such as the Doppler velocity from EarthCARE, will provide new insights into the evaluation and

One of the challenging satellite projects is the Earth Cloud, Aerosol and Radiation Explorer (EarthCARE, Illingworth et al. 2015; Wehr et al. 2023) satellite, which is a joint mission by the European Space Agencies (ESA) and Japanese Aerospace Exploration Agencies (JAXA). EarthCARE has multiple passive and active sensors in the same body to investigate clouds,

35   aerosol, precipitation, and associated radiation budgets. It has Cloud Profiling Radar (CPR), ATmospheric LIDar (ATLID), Multi Spectral Imager (MSI), and Broad Band Radiometer (BBR). The CPR of EarthCARE has the Doppler capability to obtain information on the terminal velocity of hydrometeors and vertical air motions. The multiple sensors of EarthCARE will have the opportunity to provide a synergetic understanding of the interaction between clouds and aerosols.

New observations, such as the Doppler velocity from EarthCARE, will provide new insights into the evaluation and

40   improvement of GSRMs. Before launching the satellite, it is important to understand how to use the information on the Doppler velocity to evaluate GSRMs. Therefore, we use the observation of the Doppler velocity by a cloud radar installed on the ground and investigate the methodology of evaluation of GSRMs using a sensor simulator for the Doppler velocity. We use the W-band Doppler cloud radar at Koganei-shi in Japan; this radar was installed in a similar setting to the EarthCARE CPR. We use the ground radar to understand how to use the observation by the EarthCARE CPR before the launch.

45   The ground remote sensing observation data in Japan are relatively concentrated in metropolitan areas due to disaster prevention. The ULTra-sIte for Measuring Atmosphere of Tokyo metropolitan Environment (ULTIMATE, Satoh et al. 2022) project is proposed to use these intensive observational data in the Tokyo area together with satellite observations to evaluate and improve the cloud microphysics schemes of GSRMs. Under this project, we used various types of radars, including the dual polarization Doppler C-band radars (Satoh et al. 2022, Ikuta et al. 2022), X-band polarimetric, Ka-band cloud radars, and

50   wind profilers. The W-band Doppler cloud radar at Koganei-shi is one of the radars used in the ULTIMATE project.

A satellite simulator can generate EarthCARE-like signals before the satellite launch. Roh et al. (2023) produced the EarthCARE-like radiances by a GSRM and the joint simulator for satellite sensors (Joint simulator; Hashino et al., 2013; Roh et al., 2020). The dataset is referred to as the EarthCARE synthetic data. These data were used to study the EarthCARE satellite retrieval algorithm (Hagihara et al., 2021; Wang et al., 2022; Hagihara et al., 2023). For example, Hagihara et al. (2021)

55   investigated the characteristics of the Doppler velocity using the EarthCARE synthetic data produced by Roh et al. (2023). They investigated the unfolding correction and the impact of the increase in the horizontal sampling to reduce the random errors of the Doppler velocity.

Several studies have related to the ground Doppler velocity for cloud microphysics. Han et al. (2013) evaluated the four different microphysics in the Weather Research and Forecasting (WRF) model using radar reflectivity and Doppler velocity

60   from S-band radar. Burns et al. (2016) investigated marine stratiform clouds with radar reflectivity and Doppler velocity using ground-based W-band radar and the CPR simulator (Kollias et al. 2014). However, these studies did not focus on quantitative analysis of hydrometeors for microphysics.

In this study, we develop a new evaluation method for a cloud microphysics scheme using the vertical profile of the Doppler velocity. We use the ground observation data, but the methodology can be applied to the EarthCARE observation. We evaluate two types of cloud microphysical schemes using this method. We investigate the EarthCARE-like simulations using the Joint simulator and discuss the results with different instrument settings with random errors.

The observational data and the settings of the simulation data are described in section 2. An evaluation method and results are presented in section 3. The application of the EarthCARE-like simulation data is discussed in Section 4. A summary is given in section 5.

2 Data and methodology

We used the Nonhydorstatic Icosahedral Atmospheric Model (NICAM; Satoh et al., 2014) as a GSRM. We followed the approach by Roh and Satoh (2014) to use NICAM as a regional model by transforming the grid to focus on the region of interest with high resolution (the stretched NICAM; Tomita 2008a). We conducted NICAM simulations with a G-Level 10 (GL10) horizontal resolution with the stretch-factor 100 (the ratio between the maximum and minimum grid intervals), where the minimum grid interval is approximately 800 m. We evaluated two microphysics schemes in NICAM: Single-moment Water 6-categories (Tomita 2008b) with modifications by Roh and Satoh (2014) (hereafter referred to NSW6) and the NICAM Double-moment Water 6-categories (Seiki and Nakajima 2014). The NICAM simulations were initialized with National Centers for Environmental Prediction (NECP) data with a one-degree resolution for wind, temperature, relative humidity, and geopotential data. The sea surface temperature was fixed.

We simulated two cases of rain events in September 2019. The first case (Case 1) is the tropical cyclone (TC) Faxai. The second is a weak frontal system. Case 1 of the integration and analysis time was from 00 UTC on 8 September to 00 UTC on 9 September 2019. Case 2 of the integration and analysis time was from 00 UTC on 20 September to 00 UTC on 21 September 2019.
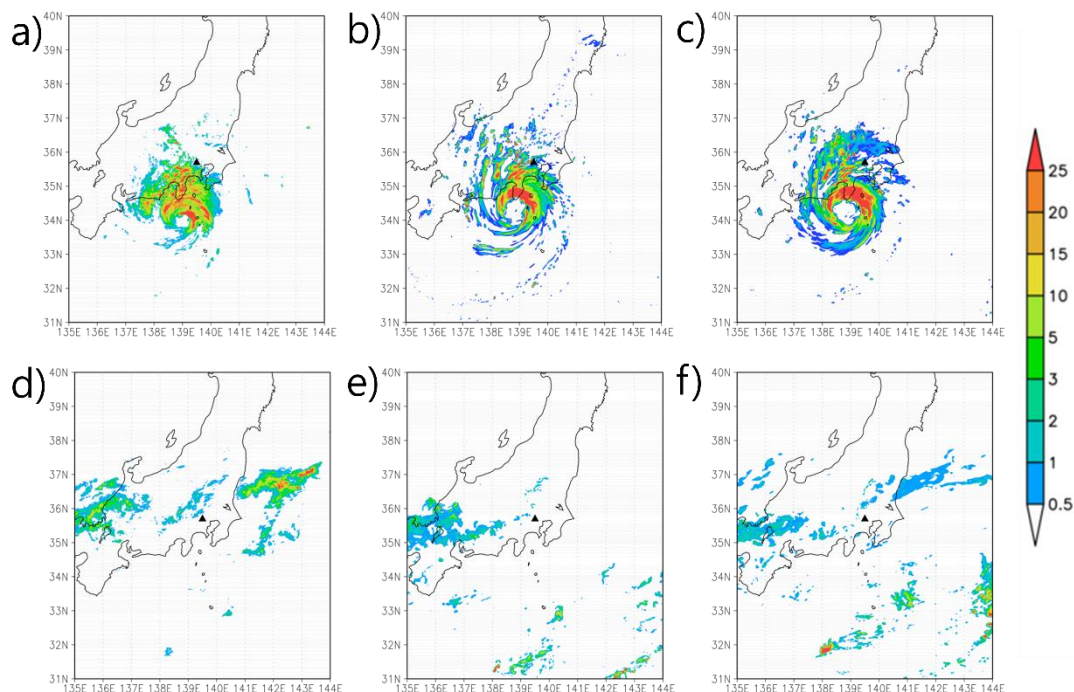
Figure 1: The horizontal distributions of the precipitation for the observation [radar/rain gauge–analyzed precipitation] (left), NSW6 (center), and NDW6 (right) simulations for Case 1 (top) and Case 2 (bottom). The black triangle indicates the location of the CPR in NICT. The contour is the precipitation amount [mm hr^{-1}].

We used the High-sensitivity Ground-based Super Polarimetric Ice-crystal Detection and Explication Radar (HG-SPIDER, Horie et al. 2000) at the National Institute of Information and Communications Technology at (35.7°N, 139.5°E). This HG-SPIDER is a vertically pointing radar and performs similarly to the EarthCARE CPR with Doppler capability. The vertical sampling resolution of HG-SPIDER is 75 m, and the observation range is 11.475 km. The time interval is much less than a second, and we used one-minute integrated data for the analysis. For Case 1, the data is only available for 12 hours.

The sensor simulators used were the EarthCARE Active Sensor Simulator (EASE, Okamoto et al. 2007, 2008; Nishizawa et al. 2008) for the evaluation of HG-SPIDER. We set the same assumptions of the size distributions of hydrometeors both for the NICAM simulation and the Joint Simulator. For cloud ice and cloud water of NSW6, size distributions are not explicitly assumed in NICAM. For these categories, we used the mono size distributions for the effective radius of cloud ice as 40 μm and the effective radius of cloud water as 8 μm in the Joint Simulator.

Figure 1 shows the horizontal distributions of precipitation for Case 1 and Case 2. Case 1 has heavy precipitation in the Tokyo metropolitan area associated with the rain bands of TC Faxai (Fig. 1a). Case 2 shows weak precipitation in the analysis area with scattered precipitation distribution (Fig. 1d). The two NICAM simulations capture the rain bands similarly to the observation for Case 1 (Fig. 1b,c) and the frontal system for Case 2 (Fig. 1e,f). For Case 1, NICAM simulated the structure

and the track of TC Faxai similarly to the observation, but the simulated TC Faxai moved faster than the observation (not shown here). For the statistical analysis, we define the analysis domain as the Japan area in Fig. 1.

3 Results

3.1 Observation by the ground CPR

110   Figure 2 shows the Contoured Frequency by Altitude Diagrams (CFADs) of the radar reflectivity and the Doppler velocity observed by the ground CPR, where constructed with 1.25 dBZ bins and 0.25 m/s bins at each height increment (75 m). For Case 1, the most probable value of the radar reflectivity rapidly decreases from the ground up to a 4 km altitude, and the maximum radar reflectivity is less than 5 dBZ. The upward decrease in the radar reflectivity is due to the strong wet attenuation from rain and the wet attenuation on the antenna's radome. Attenuation is not dominant in Case 2 because of the weaker

115   precipitation than in Case 1. The probability of the radar reflectivity has a clearer profile in Case 2. In contrast, the probability of the radar reflectivity in Case 1 does not have a meaningful structure because of the attenuation. In general, the ground observation is not free of rain attenuation, which significantly affects the radar reflectivity of the ice hydrometeors for strong precipitation.

Figure 1 shows the CFAD of the Doppler velocity. Both cases show clear vertical profiles of the maximum probability of

120   the Doppler velocity. The merit of the Doppler velocity is free to attenuation. The Doppler velocity is the sum of the terminal velocity and the vertical air motion. If we assume that the vertical air motion is relatively small, the Doppler velocity is related to the terminal velocity of the hydrometeors. A negative Doppler velocity means hydrometeors falling toward the ground, whereas a positive Doppler velocity means upward motion. Two high-frequency modes are near the melting layer at about 5 km altitude. These two modes are the fast terminal velocity of rain below 5 km and the slow terminal velocity of ice

125   hydrometeors above 5 km. In the case of heavy precipitation in Case 1, it is speculated that the riming process is dominant. It makes up more of the large and rimed ice, such as graupel and hail, with Doppler velocity less than -2 m/s in Case 1. There are high fractions above 2 m s^{-1} in Case 1 below 5 km altitude; these higher values of Doppler velocity are related to the aliasing effect with rain having a terminal velocity faster than 5.4 m/s. One must be careful about the aliasing effect for analysis of upward motion. Hereafter, we do not use radar reflectivity and only focus on the Doppler velocity evaluations.

130
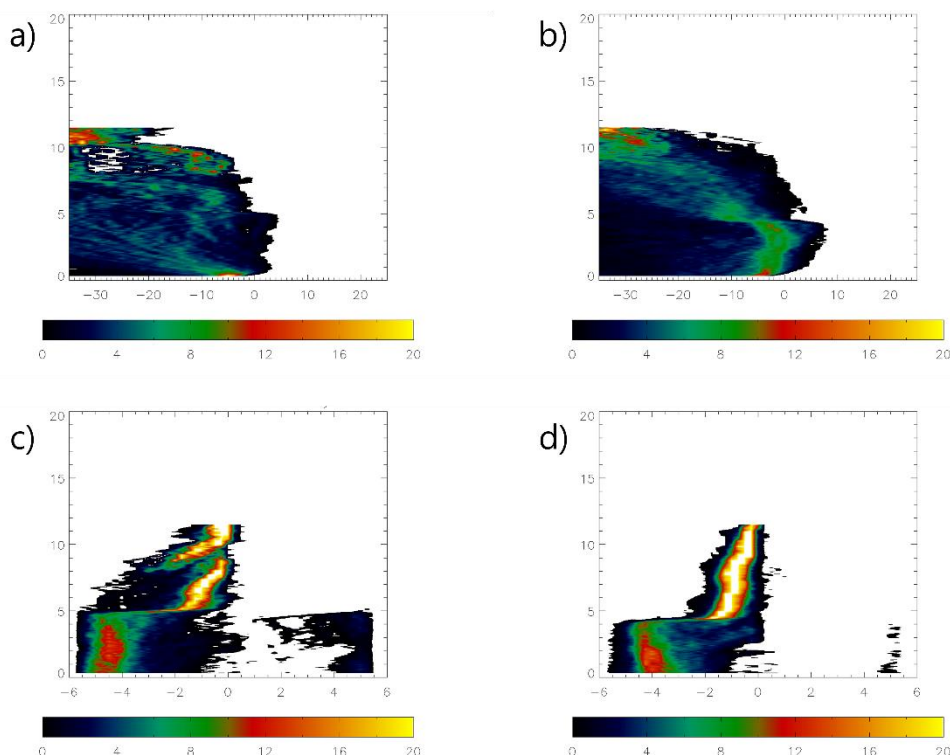
Figure 2: The CFADs of the radar reflectivities (top) and Doppler velocities (bottom) for Case 1 (left) and Case 2 (right).

3.2 Categorization of hydrometeors.

We introduce a categorization method for hydrometeors using the probability frequency of Doppler velocity in height, where was constructed with 0.25 m/s bins and 75 m bins. We identified five regimes: (1) graupel/hail, (2) cloud ice (CI)/snow, (3) rain, (4) cloud water (CW)/drizzle, and (5) upward motion using the threshold of Doppler velocity with -2 m/s, 0 m/s, and height with 5 km. We use the unfolding method based on Hagihara et al. (2021) to reduce the aliasing effect. They applied the unfolding method for the Doppler velocity above 3 m/s:

$$V_{unfoled} = V_{folded} - 2 * V_{max} \quad \text{for} \quad V_{folded} > 3\text{m/s},$$

where $V_{max} = 5.4$ m/s is for this instrument.

We have applied this method to the two cases and found the characteristics of the precipitation systems between the two cases. Note that the unfolding method is useful to reduce the aliasing effect in Case 1. The rain fraction is dominant in Case 1 (56.2%), and the CI/snow fraction is dominant in Case 2 (39.0%). The proportion of graupel/hail is higher in Case 1 (6.9%) than in Case 2 (0.3%). Because the graupel/hail fraction is large in Case 1, suggesting the importance of the riming process with convective rain. The upward motion fraction is higher in Case 1 (5.5%) than in Case 2 (1.0%), but the total fraction is

less than 6%. We can summarize that rain dominates in Case 1, while CI/snow dominates in Case 2. Using this categorizing method, we can quantify the dominant hydrometeors of the precipitation systems.

150 The thermodynamic transition height is 5 km. The maximum height of the ice-to-liquid transition is slightly lower than the melting layer (Klaassen 1988). The melting layer is lower in Case 2 than in Case 1. The melting layer depends on the seasonal variance at mid-latitude. To apply the categorization in more general cases, including the tropical area and the mid-latitudes, we will extend it by using the threshold by temperature at the freezing point 0°C instead of the height 5 km.
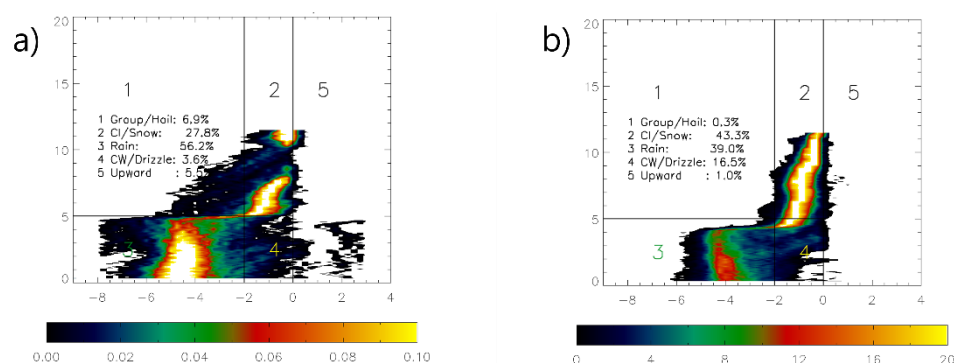
Figure 3: The categorizations of the hydrometeors using the joint histogram between Doppler velocity and height for Case 1 and Case 2.

155

3.3 Evaluation results

160 We assumed the contribution of vertical air velocity to Doppler velocity is relatively smaller than the terminal velocity of hydrometeors. If the absolute vertical air velocity is larger than the terminal velocity of hydrometeors, the categorization method makes a large bias unreliable. We investigated this issue using the NICAM simulation data. Figure 4 shows the cumulative PDFs of the absolute vertical air velocity with radar echo larger than -40 dBZ with a 0.2 m/s bin for the calculation. We found that the frequency of absolute vertical velocity above 0.2 m/s is less than 2 %, and the simulated PDF of the Doppler

165 velocity mostly depends on the cloud microphysics. NSW6 shows more contribution of the vertical air velocity on the Doppler velocity than NDW6. When we use the threshold of 2 m/s for categorizing the hydrometeors, 0.2 m/s of vertical air velocity affects the 10% bias. Case 1 has a higher fraction of the absolute vertical air velocity at faster than 0.2 m/s. Because stronger convection is produced with the tropical cyclone, the vertical velocity affects the accuracy of this categorization in NSW6. However, despite the convective cases, 2% of signals have larger than 10% of bias. Note these results are affected by the

170 horizontal resolution of the model. When we used the coarse resolution, the contribution of the vertical air motion was larger than the finer horizontal resolution (not shown).
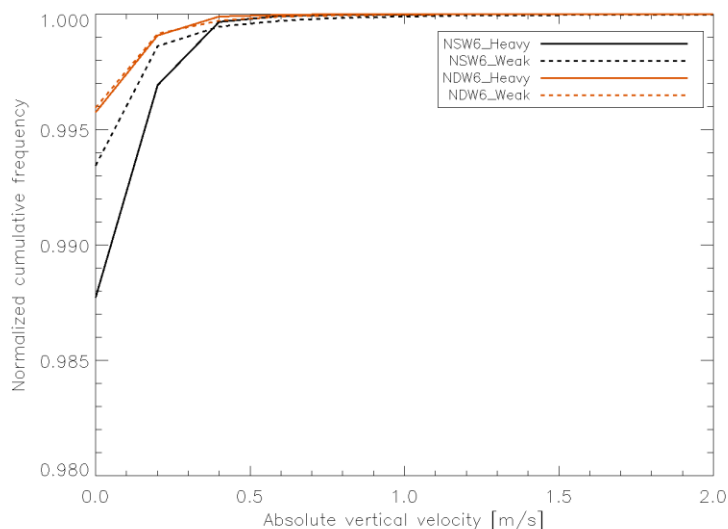
Figure 4: The cumulative PDF of the absolute vertical air velocity for the sampling data with larger than -40 dBZ in NICAM. NSW6_Heavy:
175 Case 1 with NSW6, NSW6_Weak: Case 2 with NSW6, NDW6_Heavy: Case 1 with NDW6, and NDW6_Weak: Case 2 with NDW6.

We categorize CI/snow if the terminal velocity is less than 2 m/s, and graupel/hail if the terminal velocity is greater than 2 m/s. We used the same separation threshold between rain and cloud water or drizzle. The categorization result highly depends on the cloud microphysical schemes. NSW6 and NDW6 use different terminal velocity assumptions for each ice hydrometeor
180 (Fig. 5a, b). Using 2 m/s as the threshold, NSW6 has a clear separation of the categorization between CI/snow and graupel/hail compared to NDW6. The terminal velocity of rain is similar between NSW6 and NDW6 (Fig. 5c). The drizzle with a diameter less than 0.5 mm is slower than 2 m/s of terminal velocity in both NSW6 and NDW6. The definitions of hydrometeors are different. The evaluation of the same criterion is more important than the direct comparison of hydrometeors. We can understand the effect of terminal velocity using Doppler velocity in precipitation systems.
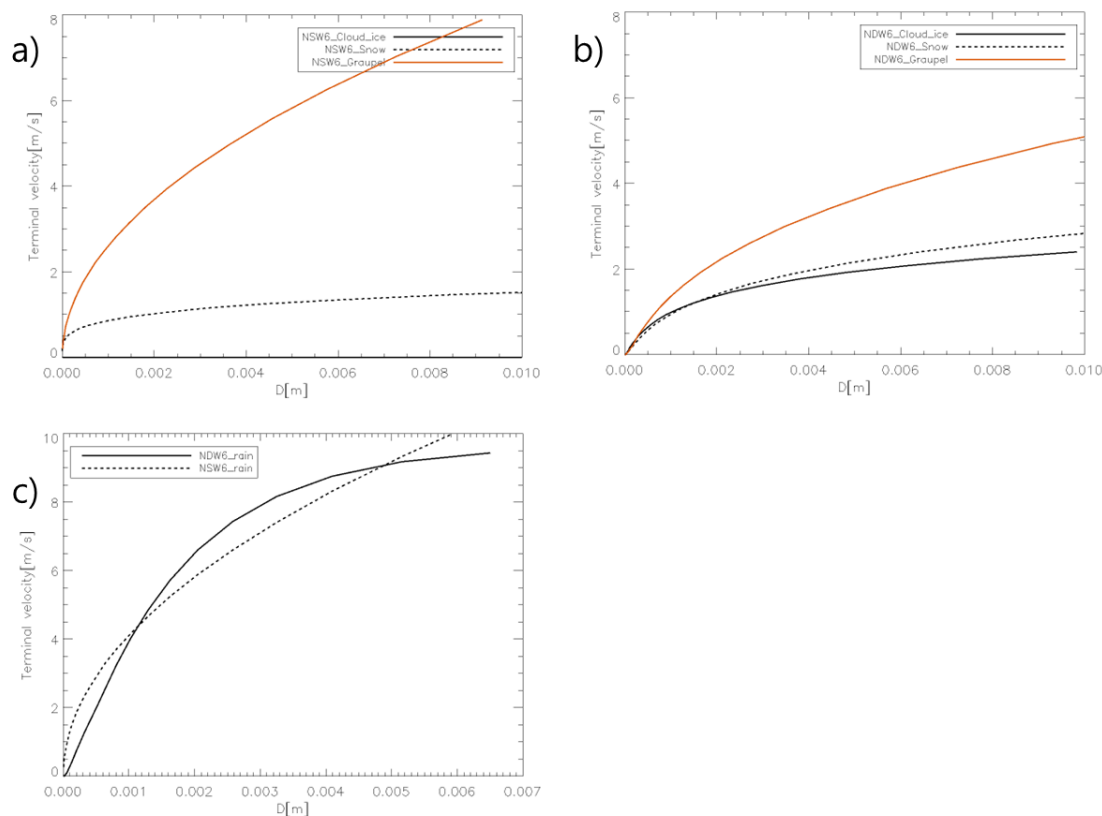
Figure 5: Terminal velocities against the diameter of ice hydrometeors in NSW6 (a) and NDW6 (b), and the diameter of rain (c).

In Figure 6, we evaluated the NICAM results using this method. We simulated the Doppler velocities for the entire analysis domain for the large data sampling. Both microphysical schemes reproduced the two branches of fast terminal velocity of rain and slow terminal velocity of ice hydrometeors as observed. The two microphysics simulations show similar case dependencies. NSW6 shows a lower graupel/hail fraction than the observation and NDW6. There is a higher fraction of graupel/hail and rain in Case 1 than in Case 2 in NSW6 and NDW6. The lower fraction of CW/drizzle in Case 1 (0.6%) than in Case 2 (3.6%) in NSW6. The choice of microphysics has a more significant effect than the case dependencies.

There are more fractions of ice hydrometeors in NDW6 than in the observation and NSW6 in Case 1. It means 63% of ice hydrometeors (graupel/hail and CI/snow) in the simulations in NDW6, but the observation is less than 35% of ice hydrometeors. We can expect a large fraction of ice hydrometeors to affect the radiation in the simulations.

The fraction of CW/drizzle is underestimated in both simulations. NDW6 performs better than NSW6. However, the two simulations do not reproduce the fraction of CW/drizzle in Case 2. One of the reasons is that the horizontal resolution is insufficient to simulate the low clouds in Case 2.

NDW6 shows the growth of snow from cloud ice more clearly than NSW6. The transition height is 9 km in Case 1 and 7 km in Case 2 in NDW6. NDW6 overestimates the graupel/hail regime associated with large snow or ice crystals. This result indicates that the terminal velocity of the snow is overestimated compared to the observation.

The melting layer is reproduced as the difference in terminal velocity between ice and liquid hydrometeors in NSW6. However, NDW6 does not show this contrast due to the high graupel/hail fraction.
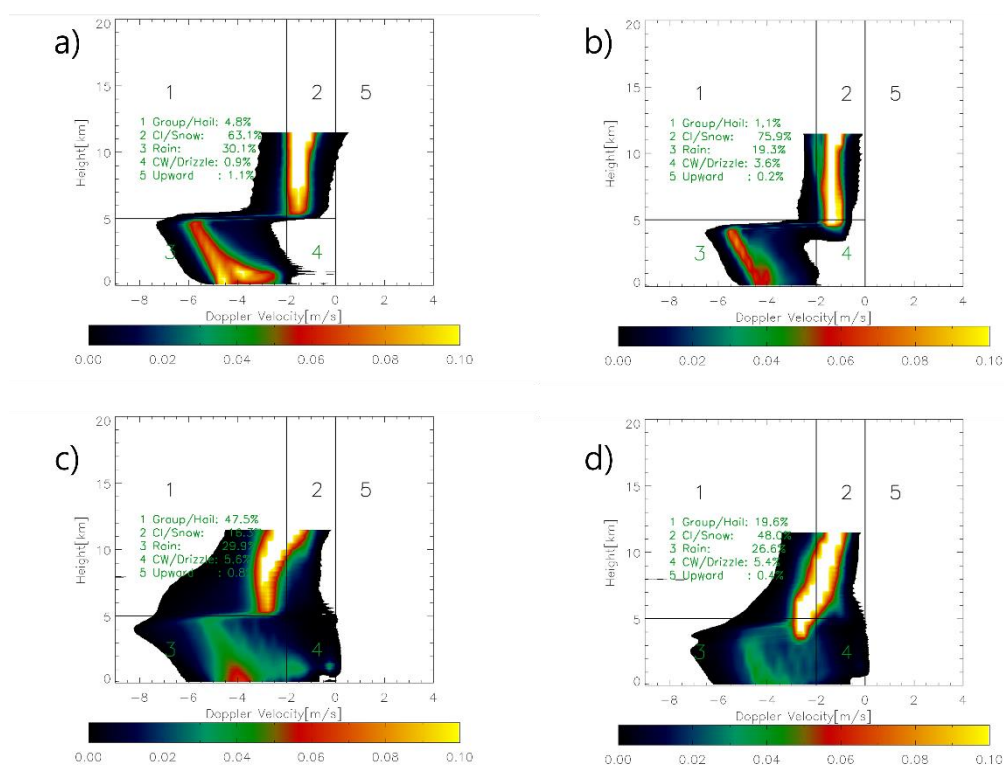
Figure 6: The categorizations of the hydrometeors in NICAM simulations for NSW6 (top) and NDW6 (bottom) in Case 1 (left) and Case 2 (right).

4 Discussions on the EarthCARE-like data

4.1 Evaluation results of the EarthCARE-like data

215   We simulated the EarthCARE-like data using NICAM and the Joint simulator. We increased the observation window to 20 km and changed the vertical resolution to 99.9308 m based on the setting of the EarthCARE CPR. We set the minimum detectable radar reflectivity to -36 dBZ. Increasing the observation window increased the sampling of ice hydrometeors. It decreased the sampling of liquid hydrometeors and upward motion (Fig. 7). Note that we changed the sign of the EarthCARE Doppler velocity so that it has the same direction as the Doppler velocity for the ground observations and we changed the bin

220   size of the height from 75 m to 99.9308 m. The accuracy of the Doppler velocity is related to the signal-to-noise ratio (SNR). We focused the sample data with a radar reflectivity greater than -15 dBZ based on Hagihara et al. (2021). In this case, we found an increase in the fraction of hail/graupel and rain regimes than all sampling data. The fraction of CI/snow is reduced compared to the other regime. The results are consistent with the ground observation data regarding case dependency related to the riming process. The characteristics of the microphysics also show a similar dependence related to the fraction of

225   graupel/hail and the fraction of CW/drizzle between NSW6 and NDW6. However, if the radar reflectivity threshold increases, the cloud echo related to small cloud ice and cloud water vanishes.
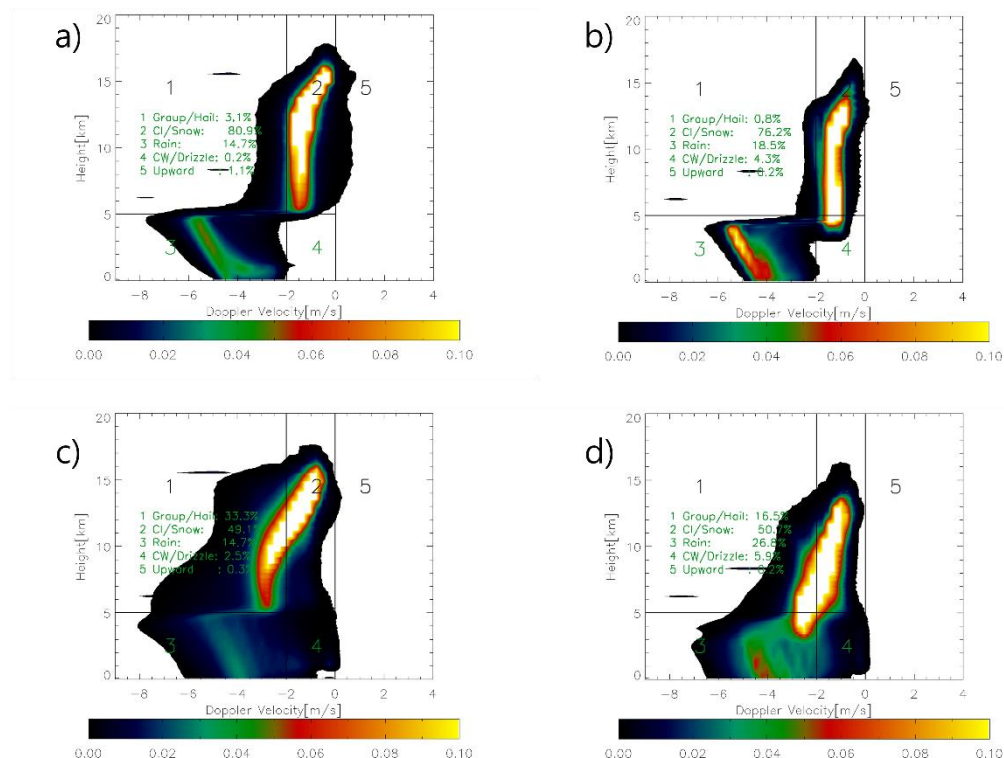
Figure 7: The categorizations of the hydrometeors based on the EarthCARE-like simulations for NSW6 (top) and NDW6 (bottom) in Case 1 (left) and Case 2 (right).

230
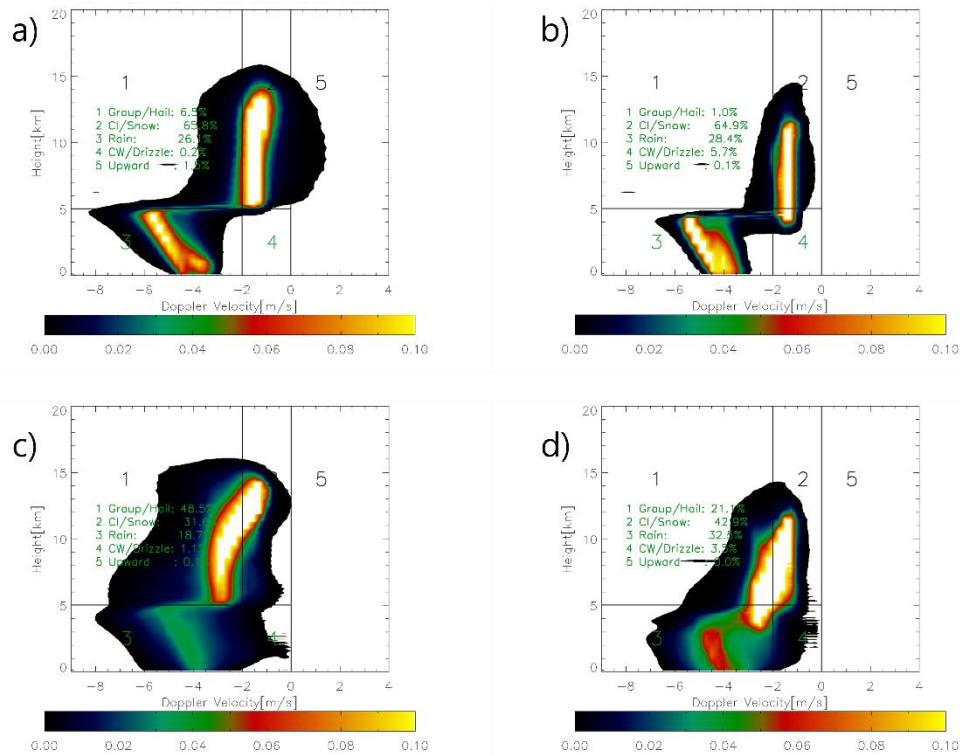
Figure 8: The same as Figure 7 but for only larger radar reflectivity than -15 dBZ.

4.2 Sensitivity tests of observation windows

The Joint simulator can simulate the signals like the EarthCARE CPR with possible random errors based on the investigation by Hagihara et al. (2021). Three modes of the observation window are considered for the EarthCARE CPR; the high, middle, and low modes observe up to the 20, 18, and 16 km altitudes at the top of the observation, respectively. The high and low modes will be used in the operation, depending on latitudes. The high mode has a higher observation window but lower Pulse Repetition Frequencies (PRFs) than the low mode. The low mode has better accuracy of Doppler velocity observation by the higher PRFs than the high mode. Figure 9 shows examples of a cross-section of Doppler velocities in Case 1, comparing the Doppler velocity with no errors, high mode errors, and low mode errors. It shows that the low mode captures Doppler velocity similarly to the true Doppler velocity, whereas the high mode hardly observes the true magnitude of Doppler velocity. Although the low mode shows better quality of the Doppler velocity observation, the observation limited to below 16 km is insufficient for the low latitude areas in the tropics.
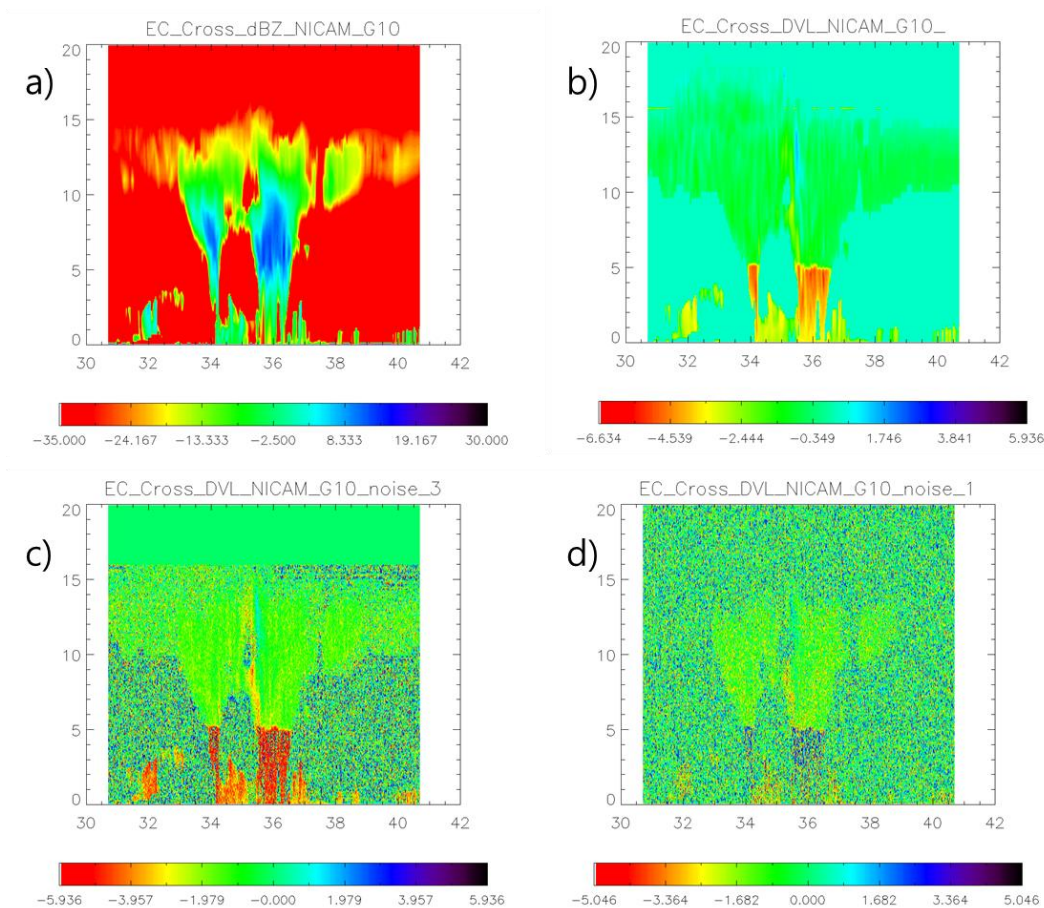
Figure 9: The cross-sections of simulated radar reflectivity (a), Doppler velocity without random error (b), Doppler velocity with the low mode (c), and Doppler velocity with the high mode for the area of Typhoon Faxai with the NICAM-NSW6 in Case 1. The contour units are dBZ for radar reflectivity (a) and m/s for Doppler velocity (b, c, d).

250

We evaluated the Doppler velocities of EarthCARE-like simulations with NSW6 and NDW6 with possible random errors based on the two observation window modes. First, we investigated the low mode results (Fig. 10). The random errors make broadening of the variance of Doppler velocity. The results are consistent with the results with no random errors in Fig. 8. The difference between Case 1 and 2 is overall similar to the signals with no error shown in Fig. 7. We see more fraction of the

255 graupel/hail regime and CW/drizzle in NDW6 than NSW6. However, there is an increase in the fraction of the graupel/hail and upward motion fraction from the broadening of variances of Doppler velocity. For the high mode, the high fractions for each regime are diverged (Fig. 11). It is hard to distinguish the characteristics of the microphysics in the high mode.

We found that random errors degraded the accuracy of the hydrometeor classification compared to the true values with no error consideration. However, the results of the low mode show similar patterns of microphysics and case dependency to the

260 true values. In this study, we did not consider the integration effect on these results. The official product of Doppler velocity

is 1 km and 10 km integrated Doppler velocity along the orbit of the EarthCARE. According to Hagihara et al. (2021), when we use a 10 km integration for cloud echoes above -15 dBZ of radar reflectivity in the high mode, the standard deviation was less than 0.5 m/s. We can expect better results using the integration method for the high mode.
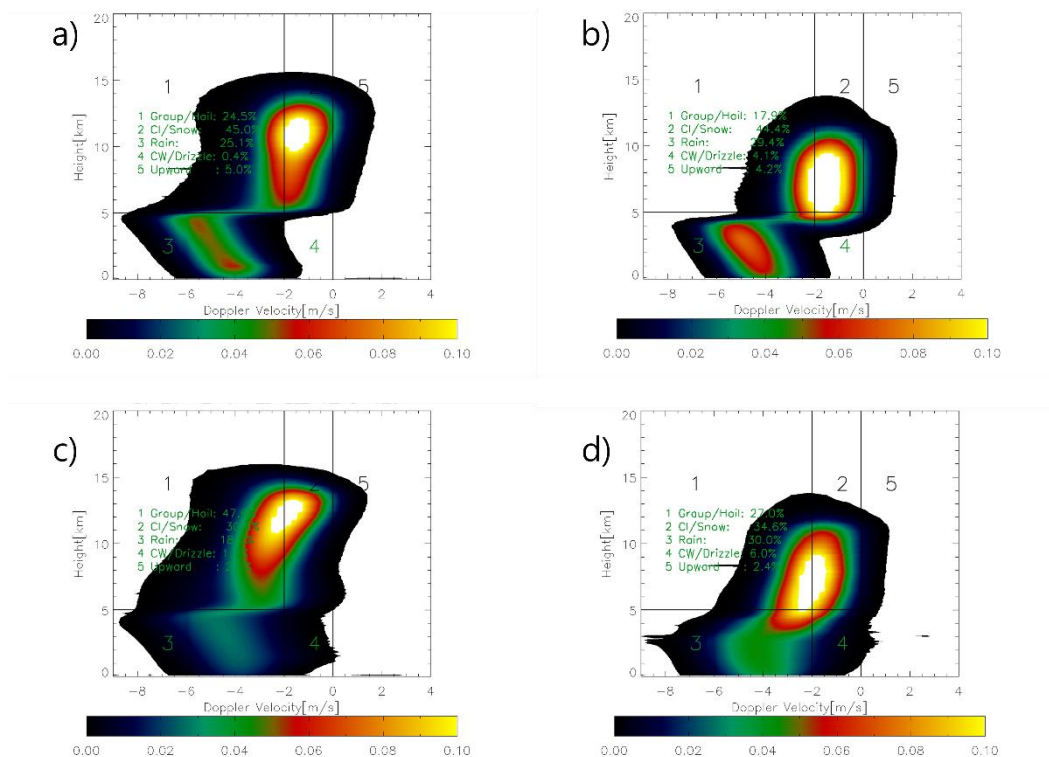
265

Figure 10: The categorizations of the hydrometeors based on the low mode of EarthCARE-like simulations for NSW6 (top) and NDW6 (bottom) in Case 1 (left) and Case 2 (right).
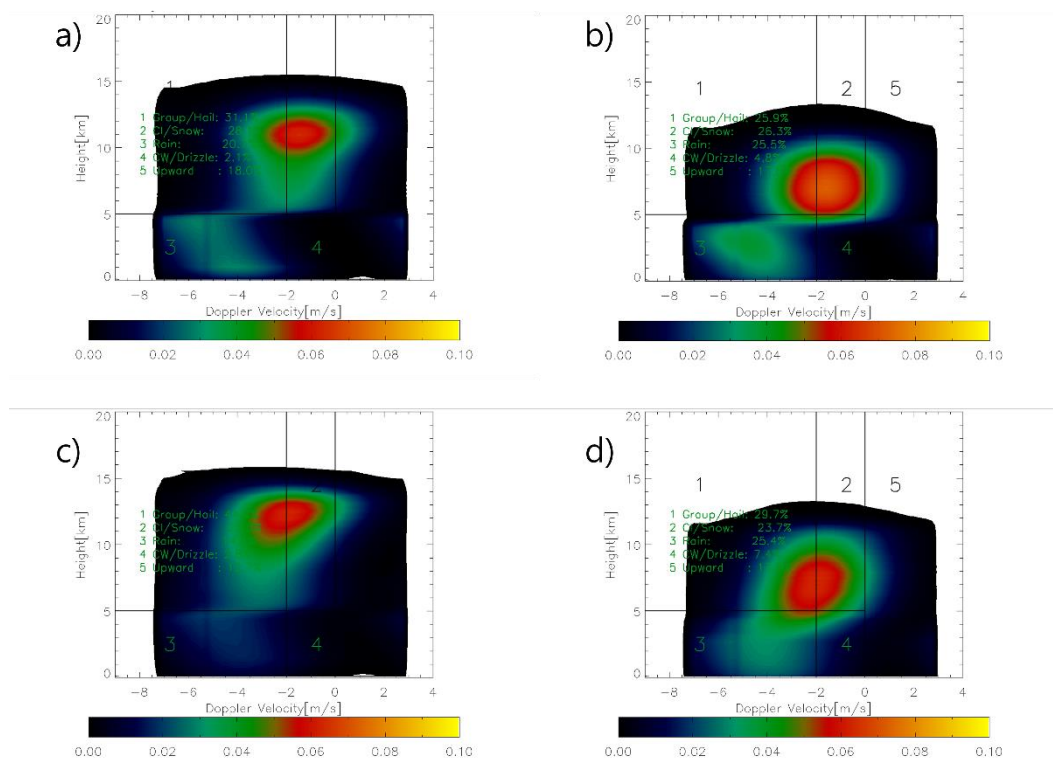
270   **Figure 11:** The categorizations of the hydrometeors based on the high mode of the EarthCARE-like simulations for NSW6 (top) and NDW6 (bottom) in Case 1 (left) and Case 2 (right).

5 Summary

In this study, we developed the methodology of using the Cloud Profiling Radar (CPR) of Earth Cloud, Aerosol and
275   Radiation Explorer (EarthCARE) before the launch of EarthCARE in 2024 for model evaluations. We analyzed observation data by the ground-based CPR for two cases with different precipitation events in September 2019. By using the observed data, we compared simulated results for these cases by the stretched version of the global non-hydrostatic model, NICAM, with two different cloud microphysics schemes.

We introduced the categorization method of the hydrometeors for analyzing Doppler velocity observed by CPR. This method
280   is based on the probability frequency of Doppler velocity with respect to heights. We identified five regimes: (1) graupel/hail, (2) cloud ice (CI)/snow, (3) rain, (4) cloud water (CW)/drizzle, and (5) upward motion. This method clarifies the contribution of the hydrometeors to the precipitation systems and characterize cloud microphysics. For the case of the tropical cyclone with heavy precipitation, the rain and graupel/hail fraction are more dominant than the weak precipitation case.

We applied the Joint simulator to the NICAM simulation data with two cloud microphysics schemes and analyzed the
285   simulated Doppler velocity data using this categorizing method. These simulations produced a similar horizontal distribution
of precipitation to the observation. The cloud microphysics schemes strongly impact the probability frequency of Doppler
velocity in terms of heights, particularly for the heavy precipitation case. The double moment scheme reproduced a higher
fraction of the graupel/hail regime than the observation and the single moment scheme.

The advantage of the use of Doppler velocity in the categorization of the hydrometeors is that Doppler velocities suffer less
290   impact from the attenuation of rain and wet attenuation on an antenna. The ground CPR observation of the radar reflectivity
for the precipitation case is limited because of wet attenuation on an antenna. The Doppler velocity of the ground observation
is more reliable than the radar reflectivity. Doppler velocities are from the terminal velocity of the hydrometeors and vertical
air motion. We found the main contribution to Doppler velocities is the terminal velocity of hydrometeors by analysis of
simulation results. The terminal velocity has information about the density and thermodynamics phases of hydrometeors.

295   We expanded this evaluation method using the simulated Doppler velocities of the EarthCARE satellite. The results were
consistent with the ground observation data. The maximum observation height of the EarthCARE CPR was higher than the
ground observation. We took a test about the threshold of radar reflectivity with -15 dBZ for the Doppler velocity. The results
were consistent with the ground observation data. However, there was an increase of fraction with ice hydrometeors and a
decrease of the CW/drizzle because of the increase of the observation range and the threshold of the radar reflectivity.

300   We considered the observation windows and random errors associated with the Pulse Repetition Frequencies (PRFs). When
we added the random error based on the observation window, the Doppler velocities diverged from the results without error.
The 16 km observation window mode has the higher PRFs and reproduced consistent results similarly to the results without
error. The differences between the two cloud microphysics schemes were apparent, such as the difference between the ground
observation and the simulation with the 16 km observation window. In contrast, the 20 km observation window produces more
305   random errors, and it was difficult to distinguish the different characteristics between the two cloud microphysics. For the
evaluation of cloud microphysics, the 16 km observation window is preferable, but higher clouds than the 16 km altitude would
be no longer omitted over the tropical region. We need to discuss the unseen cloud fraction near tropical regions.

The merit of the CPR observation from space is to get better radar reflectivity for ice hydrometeors because of no attenuation
from liquid hydrometeors than the ground observation data. The combination of the radar reflectivity and Doppler velocity has
310   more information about the maximum size and terminal velocity of ice hydrometeors. The EarthCARE has other thee
instruments: ATLID, MSI, and BBR. These instruments can detect the different information related to cloud and precipitation
systems.

In this study, the observation data is located in the middle latitude. The melting layer changes between the two cases and
the categorization between the ice and liquid hydrometeors has a bias because of the different melting layer heights. We will
315   improve the transition height in the future for the middle latitude.

After the launch of the EarthCARE satellite, the Doppler velocity can be available over the globe. The Doppler velocity is
more directly related to the terminal velocity of hydrometeors and characterizes the cloud microphysics. The simulated vertical

distribution of hydrometeors of GSRMs is highly divergent under the current intercomparison of the DYAMOND project (Roh et al. 2021). To improve GSRMs, the vertical distribution of hydrometeors must be more realistic by referring to available
320 observations. The categorization method proposed in this study will quantify the hydrometeors simulated by GSRMs and lead to their improvement.

Data availability

The Joint-Simulator is available from https://www.eorc.jaxa.jp/theme/Joint-Simulator/userform/js_userform.html.
325

Author contributions

WR drafted the manuscript, and produced the NICAM simulation and simulated Doppler velocity using the Joint simulator. MS contributed the NICAM data and the manuscript. YH developed the random error model based on the observation window. HH and YO worked on the W-band observation in NICT. TK led the Joint-Simulator development and provided feedback on
330 the manuscript draft.

Competing interests

The authors declare that they have no conflicts of interest.

Acknowledgements

The authors thank members of the JAXA EarthCARE Science Team and the Joint-Simulator project. The authors also thank
335 to ESA for providing the measured value of response functions of EarthCARE/MSI. The authors thank Dr. Toshi Matsui for providing the orbit/scan simulator. Computational resources were partly provided by the National Institute for Environmental Studies.

Financial support

This work was supported by the EarthCARE satellite study commissioned by the Japan Aerospace Exploration Agency. MS
340 and WR were supported by a Grant-in-Aid for Scientific Research B (20H01967) and the Program for Promoting Technological Development of Transportation of the Ministry of Land, Infrastructure, Transport, and Tourism (MLIT).

References

345

Burns, D., Kollias, P., Tatarevic, A., Battaglia, A., and Tanelli, S.: The performance of the EarthCARE Cloud Profiling Radar in marine stratiform clouds. *Journal of Geophysical Research: Atmospheres*, *121*(24), 14-525, 2016

Hagihara, Y., Ohno, Y., Horie, H., Roh, W., Satoh, M., Kubota, T., and Oki, R.: Assessments of Doppler velocity errors of EarthCARE cloud profiling radar using global cloud system resolving simulations: Effects of Doppler broadening and folding,

350   IEEE Trans. Geosci. Remote Sens., 60, 1–9, https://doi.org/10.1109/TGRS.2021.3060828, 2021.

Hagihara, Y., Ohno, Y., Horie, H., Roh, W., Satoh, M., and Kubota, T.: Global evaluation of Doppler velocity errors of EarthCARE Cloud Profiling Radar using global storm-resolving simulation, EGUsphere [preprint], https://doi.org/10.5194/egusphere-2022-1255, 2023.

Han, M., Braun, S. A., Matsui, T., and Williams, C. R.: Evaluation of cloud microphysics schemes in simulations of a winter

355   storm using radar and radiometer measurements. *Journal of Geophysical Research: Atmospheres*, *118*(3), 1401-1419, 2013

Hashino, T., Satoh, M., Hagihara, Y., Kubota, T., Matsui, T., Nasuno, T., and Okamoto, H.: Evaluating cloud microphysics from NICAM against CloudSat and CALIPSO, J. Geophys. Res. Atmos., 118, 7273–7292, https://doi.org/10.1002/jgrd.50564, 2013.

Horie, H., Iguchi, T., Hanado, H., Kuroiwa, H., Okamoto, H., & Kumagai, H.: Development of a 95-GHz airborne cloud

360   profiling radar (SPIDER)—Technical aspects--. *IEICE transactions on communications*, *83*(9), 2010-2020, 2000

Ikuta, Y., Satoh, M., Sawada, M., Kusabiraki, H., Kubota, T.: Improvement of the cloud microphysics scheme of the mesoscale model at the Japan Meteorological Agency using space-borne radar and microwave imager of the Global Precipitation Measurement as reference. Mon. Wea. Rev., 149, 3803-3819, https://doi.org/10.1175/MWR-D-21-0066.1, 2021.

Ikuta, Y., Sawada, M., Satoh, M.: Determining the impact of boundary layer schemes on the secondary circulation of Typhoon

365   FAXAI using radar observations in the gray zone. J. Atmos. Sci., 81, 961–981. https://doi.org/10.1175/JAS-D-22-0169.1, 2022.

Illingworth, A. J., Barker, H. W., Beljaars, A., Ceccaldi, M., Chepfer, H., Clerbaux, N., Cole, J., Delanoë, J., Domenech, C., Donovan, D. P., Fukuda, S., Hirakata, M., Hogan, R. J., Huenerbein, A., Kollias, P., Kubota, T., Nakajima, T., Nakajima, T. Y., Nishizawa, T., Ohno, Y., Okamoto, H., Oki, R., Sato, K., Satoh, M., Shephard, M. W., Velázquez-Blázquez, A., Wandinger, U., Wehr, T., and Van Zadelhoff, G. J.: The EarthCARE satellite: The next step forward in global measurements of clouds,

370   aerosols, precipitation, and radiation, Bull. Am. Meteorol. Soc., 96, 1311–1332, https://doi.org/10.1175/BAMS-D-12-00227.1, 2015.

Klaassen, W.: Radar observations and simulation of the melting layer of precipitation. *Journal of Atmospheric Sciences*, *45*(24), 3741-3753, 1988.

Kollias, P., Tanelli, S., Battaglia, A., and Tatarevic, A.: Evaluation of EarthCARE cloud profiling radar Doppler velocity

375   measurements in particle sedimentation regimes. *Journal of Atmospheric and Oceanic Technology*, *31*(2), 366-386, 2014

Kollias, P., Battaglia, A., Tatarevic, A., Lamer, K., Tridon, F., and Pfitzenmaier, L.: The EarthCARE cloud profiling radar (CPR) doppler measurements in deep convection: challenges, post-processing, and science applications. Remote sensing of the atmosphere, clouds, and precipitation *VII*, SPIE, 57-68, 2018

Nishizawa, T., Okamoto, H., Takemura, T., Sugimoto, N., Matsui, I., & Shimizu, A.: Aerosol retrieval from two-wavelength

380 backscatter and one-wavelength polarization lidar measurement taken during the MR01K02 cruise of the R/V Mirai and evaluation of a global aerosol transport model, J. Geophys. Res., 113, D21201, https://doi.org/10.1029/2007JD009640, 2008.

Okamoto, H., Nishizawa, T., Takemura, T., Kumagai, H., Kuroiwa, H., Sugimoto, N., ... & Nakajima, T.: Vertical cloud structure observed from shipborne radar and lidar,: mid-latitude case study during the MR01/K02 cruise of the R/V Mirai, J. Geophys. Res, 112, D08216, https://doi.org/10.1029/2006JD007628, 2007.

385 Okamoto, H., Nishizawa, T., Takemura, T., Sato, K., Kumagai, H., Ohno, Y., ... & Nakajima, T.: Vertical cloud properties in the tropical western Pacific Ocean: Validation of the CCSR/NIES/FRCGC GCM by shipborne radar and lidar, J. Geophys. Res., 113, D24213. https://doi.org/10.1029/2008JD009812, 2008.

Roh, W. and Satoh, M.: Evaluation of precipitating hydrometeor parameterizations in a single-moment bulk microphysics scheme for deep convective systems over the tropical central Pacific, J. Atmos. Sci., 71, 2654–2673,

390 https://doi.org/10.1175/JAS-D-13-0252.1, 2014.

Roh, W., Satoh, M., and Nasuno, T.: Improvement of a cloud microphysics scheme for a global nonhydrostatic model using TRMM and a satellite simulator, J. Atmos. Sci., 74, 167–184, https://doi.org/10.1175/JAS-D-16-0027.1, 2017.

Roh, W. and Satoh, M.: Extension of a multisensor satellite radiance-based evaluation for cloud system resolving models, J. Meteor. Soc. Japan, 96, 55–63, https://doi.org/10.2151/jmsj.2018-002, 2018.

395 Roh, W., Satoh, M., Hashino, T., Okamoto, H., and Seiki, T.: Evaluations of the thermodynamic phases of clouds in a cloud-system-resolving model using CALIPSO and a satellite simulator over the Southern Ocean, J. Atmos. Sci., 77, 3781–3801, https://doi.org/10.1175/JAS-D-19-0273.1, 2020.

Roh, W., Satoh, M., & Hohenegger, C.: Intercomparison of cloud properties in DYAMOND simulations over the Atlantic Ocean. *Journal of the Meteorological Society of Japan. Ser. II*, *99*(6), 1439-1451, 2021

400 Roh, W., Satoh, M., Hashino, T., Matsugishi, S., Nasuno, T., and Kubota, T.: The JAXA EarthCARE synthetic data using a global storm resolving simulation. https://doi.org/10.5281/zenodo.7835229. 2023.

Satoh, M., Matsuno, T., Tomita, H., Miura, H., Nasuno, T., and Iga, S.: Nonhydrostatic icosahedral atmospheric model (NICAM) for global cloud resolving simulations, J. Comput. Phys., 227, 3486–3514, https://doi.org/10.1016/j.jcp.2007.02.006, 2008.

405 Satoh, M., Tomita, H., Yashiro, H., Miura, H., Kodama, C., Seiki, T., Noda, A. T., Yamada, Y., Goto, D., Sawada, M., Miyoshi, T., Niwa, Y., Hara, M., Ohno, T., Iga, S., Arakawa, T., Inoue, T., and Kubokawa, H.: The Non-hydrostatic Icosahedral Atmospheric Model: description and development, Prog. Earth Planet. Sci., 1, 18. doi:10.1186/s40645-014-0018-1, 2014.

Satoh, M., Stevens, B., Judt, F., Khairoutdinov, M., Lin, S. J., Putman, W. M., & Düben, P.: Global cloud-resolving models. *Current Climate Change Reports*, *5*, 172-184, 2019.

410   Satoh, M., Matsugishi, S., Roh, W., Ikuta, Y., Kuba, N., Seiki, T., ... and Okamoto, H.: Evaluation of cloud and precipitation processes in regional and global models with ULTIMATE (ULTra-sIte for Measuring Atmosphere of Tokyo metropolitan Environment): a case study using the dual-polarization Doppler weather radars. *Progress in Earth and Planetary Science*, *9*(1), 1-28, 2022

Seiki, T., and Nakajima, T.: Aerosol effects of the condensation process on a convective cloud simulation. *Journal of the*
415   *Atmospheric Sciences*, *71*(2), 833-853, 2014.

Stevens, B., Satoh, M., Auger, L., Biercamp, J., Bretherton, C. S., Chen, X., ... & Zhou, L.: DYAMOND: the DYnamics of the Atmospheric general circulation Modeled On Non-hydrostatic Domains, Prog. Earth Planet. Sci., 6, https://doi.org/10.1186/s40645-019-0304-z, 2019.

Tomita, H.: A stretched icosahedral grid by a new grid transformation. *J. Meteorol.l Soc. Jpn.*, **86,** 107–119, 2008a

420   Tomita, H.: New microphysical schemes with five and six categories by diagnostic generation of cloud ice. *J. Meteorol. Soc. Jpn.*, **86,** 121–142, 2008b

Wang, M., Nakajima, T. Y., Roh, W., Satoh, M., Suzuki, K., Kubota, T., and Yoshida, M.: Evaluation of the smile effect on the Earth Clouds, Aerosols and Radiation Explorer (EarthCARE)/Multi-Spectral Imager (MSI) cloud product, EGUsphere [preprint], https://doi.org/10.5194/egusphere-2022-736, 2022.

425   Wehr, T., Kubota, T., Tzeremes, G., Wallace, K., Nakatsuka, H., Ohno, Y., ... & Bernaerts, D.: The EarthCARE Mission– Science and System Overview. *EGUsphere*, *2023*, 1-47, 2023